Chem Circularity

Article

Enzyme-mediated consolidation of lignocellulosic materials with a flame-retardant and fully recyclable mineral binder

Graphical abstract

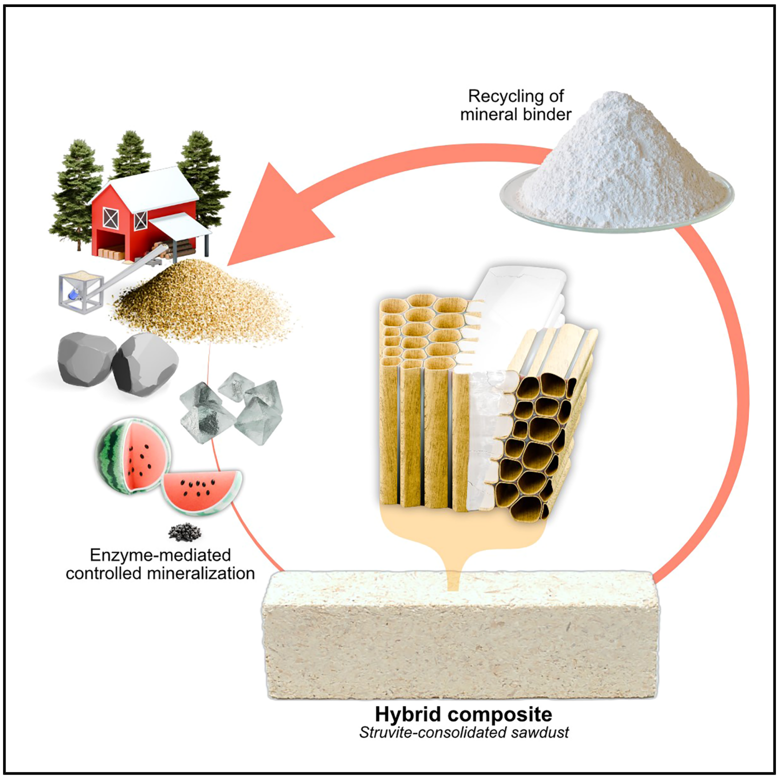

Highlights

- Recyclable mineral binder consolidates sawdust into robust hybrid composites
- Enzyme-mediated phase transformation allows controlled struvite crystallization
- Hybrid composites show excellent fire resistance at low binder content
- Binder recovery under mild aqueous conditions enables circular materials economy

Authors

Ronny Kürsteiner, Dan Vivas Glaser, Maximilian Ritter, ..., Federico Carosio, Ingo Burgert, Guido Panzarasa

Correspondence

ronnyk@ethz.ch (R.K.),
iburgert@ethz.ch (I.B.),
guidop@ethz.ch (G.P.)

In brief

An enzymatically induced phase transformation allows the controlled crystallization of struvite as a mineral binder for the consolidation of lignocellulosic by-products. This mineralization approach under confinement leads to large crystals that interlock with wood particles, forming hybrid composites with high compressive strength and excellent fire resistance even at low binder content. The mineral binder can be fully recovered under mild aqueous conditions without loss of performance, a significant step toward a circular materials economy.

Kürsteiner et al., 2026, Chem Circularity *1*, 100004

https://doi.org/10.1016/j.checir.2025.100004

Please cite this article in press as: Kürsteiner et al., Enzyme-mediated consolidation of lignocellulosic materials with a flame-retardant and fully recyclable mineral binder, Chem Circularity (2025), https://doi.org/10.1016/j.checir.2025.100004

Chem Circularity

CellPress
OPEN ACCESS

Article

Enzyme-mediated consolidation of lignocellulosic materials with a flame-retardant and fully recyclable mineral binder

Ronny Kürsteiner,[1,5,*] Dan Vivas Glaser,[1] Maximilian Ritter,[1,2] Annapaola Parrilli,[3] Jonas Garemark,[1] Lorenza Maddalena,[4] Thomas Schnider,[1] Christopher H. Dreimol,[1,2] Federico Carosio,[4] Ingo Burgert,[1,2,*] and Guido Panzarasa[1,*]

[1]Wood Materials Science, Institute for Building Materials, ETH Zurich, 8093 Zurich, Switzerland
[2]WoodTech, Cellulose & Wood Materials, Empa, 8600 Dübendorf, Switzerland
[3]Center for X-ray Analytics, Empa, 8600 Dübendorf, Switzerland
[4]Dipartimento di Scienza Applicata e Tecnologia, Politecnico di Torino - Sede di Alessandria, 15121 Alessandria, Italy
[5]Lead contact
*Correspondence: ronnyk@ethz.ch (R.K.), iburgert@ethz.ch (I.B.), guidop@ethz.ch (G.P.)

https://doi.org/10.1016/j.checir.2025.100004

CONTEXT & SCALE Sawdust is a major lignocellulosic by-product of the wood-processing industry, and millions of tons of it get downcycled by incineration every year. This study investigates the upcycling of softwood sawdust by means of struvite, resulting in inorganically bound hybrid materials with functional properties. The use of ureolytic protein bodies extracted from watermelon seeds, an agricultural by-product, allows for control of struvite crystallization, forming large crystals. As a result, the sawdust is efficiently consolidated even at a low struvite-to-sawdust ratio of 0.65 by weight. The struvite crystals conform to the rough surface topography of the sawdust and grow into accessible lumina (pores in the wood structure), leading to strong mechanical interlocking. The resulting composites are mechanically robust with a compressive strength of ~4.5 MPa at ~780 kg m^{-3} independent of the sawdust particle size. Struvite is an active inorganic flame retardant, and its homogeneous distribution in the hybrid composite confers outstanding flame-retardant behavior to the material and a fire-shielding ability as a result of efficient char-layer formation. The material could find application in internal walls because of its excellent fire protection and, after use, could be re-used for soil remediation given that struvite acts as a slow-release fertilizer. Alternatively, the struvite binder can be fully recycled under mild aqueous conditions while retaining its mechanical performance, marking a significant step toward a circular materials economy. The recovered sawdust could then be burned for energy generation (as it was originally destined) or potentially used for the fabrication of new composites. The mild conditions required for the binder recovery make the recycling of spent composites feasible and facilitate the use of alternative struvite sources, such as precipitates from wastewater facilities, as precursor materials.

SUMMARY

The wood industry produces enormous quantities of lignocellulosic by-products, such as sawdust, and their incineration for energy recovery results in substantial carbon emissions and the loss of valuable raw materials. Here, we introduce struvite as a fully recyclable inorganic binder for the consolidation of sawdust into high-performance hybrid materials. The mineral binder is produced *in situ* by an enzymatically induced solution-mediated phase transformation driven by ureolytic protein bodies extracted from watermelon seeds. The resulting material exhibits excellent fire resistance with a long time to ignition (51 ± 1 s), low peak heat release (118 ± 2 kW m^{-2}), and fast flame self-extinction due to efficient char-layer formation. Moreover, it displays high compressive strength (4.71 ± 0.37 MPa). Crucially for sustainability, the struvite binder can be recovered under mild aqueous conditions without loss of performance, offering a valid path toward a circular materials economy.

Please cite this article in press as: Kürsteiner et al., Enzyme-mediated consolidation of lignocellulosic materials with a flame-retardant and fully recyclable mineral binder, Chem Circularity (2025), https://doi.org/10.1016/j.checir.2025.100004

INTRODUCTION

Wood is a versatile and abundant construction material combining a high inherent strength-to-weight ratio with high local availability. However, its conventional industrial processing produces substantial quantities of by-products.[1] Although some of these can be used for further processing, such as in the pulp and paper or particle board industry, a considerable portion, notably sawdust, is often burned as fuel.[2,3] To avoid its downcycling, sustainable strategies must integrate sawdust into the materials stream, for example, by consolidating it into high-performance composites. However, the binders used for consolidating low-grade wood by-products can introduce significant environmental burdens. Traditional polymeric binders, such as formaldehyde-based resins, polyolefins, and polyvinyl chloride, are generally derived from finite fossil resources and are not suitable for recycling. Consequently, if they end up in landfills, they can pose a long-term pollution risk as a result of the formation of microplastics or harmful degradation products, affecting both terrestrial and aquatic ecosystems.[4–6] In addition, fire safety remains a major concern for wood-based composites.[7] Compared with polymeric ones, inorganic binders can offer great advantages in terms of resistance to fire.[8–11] However, the production of inorganic precursors is most often energy intensive because of the high temperatures required, e.g., during calcination, and most mineral binders are non-recyclable.[12] Hence, it is necessary to find novel mineral-based binding strategies that prioritize sustainability, fire safety, and robustness.

The use of struvite ($MgNH_4PO_4 \cdot 6H_2O$) as a fire-retardant mineral phase for the functionalization of bulk wood was previously investigated by Guo et al.,[13,14] who demonstrated its promise as an alternative to toxic boron-based and water-soluble ammonium-phosphate-based fire retardants. Upon heating, struvite decomposes endothermically under the release of water vapor and ammonia, forming mesoporous magnesium phosphate.[15] Differential thermogravimetric analysis (DTGA) showed that the major mass-loss peaks depend strongly on the heating rate and are 104°C and 190°C for heating rates of 1°C and 20°C min^{-1}, respectively.[16] This endothermic process lowers the surface temperature of the material and leads to a blanketing and dilution effect as a result of the volatiles released. Compared with those of unmodified spruce, the pyrolysis products of struvite-mineralized spruce showed a drastically lower total abundance in evolved volatiles and an increase in evolved levoglucosenone, promoting char formation.[14] The most important metric in the assessment of flame-retardant building materials is the heat release rate (HRR),[17] which measures the heat released by the material as it undergoes (forced) combustion. In materials research, the HRR, alongside the time to ignition (TTI) and the smoke production rate,[18] is assessed by forced-combustion tests using a cone calorimeter (which measures the reaction of the material to an external heat source), and these conditions are widely used as a standardized proxy for early-stage fire exposure.[19] In addition to the calorimetric assay, more qualitative flammability tests can evaluate a sample's reaction to direct flame exposure.

Here, we introduce struvite as a recyclable mineral binder for consolidating sawdust into robust and highly flame-retardant composites through an innovative processing approach (Figure 1). Conventional precipitation methods result in uncontrolled struvite nucleation, leading to the formation of small crystallites.[20,21] This results in mechanically weak composites, especially with lignocellulosic substrates, given that the materials must be able to accommodate significant stresses resulting from the dimensional changes caused by varying moisture content, both upon drying after composite formation and from changes in relative humidity (RH). By contrast, we use an enzymatically induced solution-mediated phase transformation (SMPT) to synthesize struvite under confinement. Ureolytic protein bodies (UPBs), extracted from watermelon seeds, hydrolyze urea in the presence of sodium sulfate, allowing control of the crystallization process and resulting in large struvite crystals that intimately template the sawdust surface. This strong mechanical interlocking of the wood-mineral interface allows the formation of robust composites with a struvite-to-sawdust ratio of 0.65 (by weight) regardless of the size of the sawdust particles used. Unidirectional compaction during fabrication induces a preferential alignment of sawdust particles perpendicular to the direction of compaction, leading to an anisotropy in mechanical properties. This anisotropy was assessed under different loading directions and found to correlate with particle orientation quantified by X-ray microtomography, as evidenced by a ~50% increase in compressive strength in the direction of compaction (~4.5 vs. ~3.0 MPa). Furthermore, the composites show excellent flame-retardant properties. Finally, we demonstrate that the struvite binder can be recycled under very mild conditions and that the composites made with the reclaimed binder show properties comparable to those of native ones. Our process has the potential to be integrated directly into a circular economic framework.

RESULTS AND DISCUSSION

Solution-mediated phase transformation

Wood-mineral hybrid composites combine organic lignocellulosic materials with inorganic mineral phases to form enhanced, multifunctional materials. Producing composites with low overall mineral content requires strategies that ensure uniform mineral phase deposition within the wood matrix while minimizing water usage. Effective sawdust consolidation relies on bringing particles into close proximity and using small volumes of highly concentrated precursor solutions to achieve sufficient mineral loading. However, direct precipitation from aqueous solution is limited by the low solubility of magnesium phosphates, including struvite ($MgNH_4PO_4 \cdot 6H_2O$) and newberyite ($MgHPO_4 \cdot 3H_2O$).[22] To circumvent this issue, we exploited the property of newberyite to undergo a SMPT into struvite. This process relies on shifting the equilibrium of a newberyite suspension toward struvite formation by increasing both pH and ammonium ion concentration.[23] Upon the addition of NH_4^+ at elevated pH, newberyite undergoes gradual dissolution while struvite simultaneously crystallizes. This approach of introducing the mineral precursor as a suspension rather than as a solution allowed us to significantly increase the precursor concentration, enabling higher sawdust loadings and ensuring sufficient mineral-phase formation for robust consolidation.

The direct addition of ammonium carbonate to rapidly increase both pH and ammonium ion concentration resulted in uncontrolled, fast struvite nucleation, yielding smaller crystallites

Please cite this article in press as: Kürsteiner et al., Enzyme-mediated consolidation of lignocellulosic materials with a flame-retardant and fully recyclable mineral binder, Chem Circularity (2025), https://doi.org/10.1016/j.checir.2025.100004

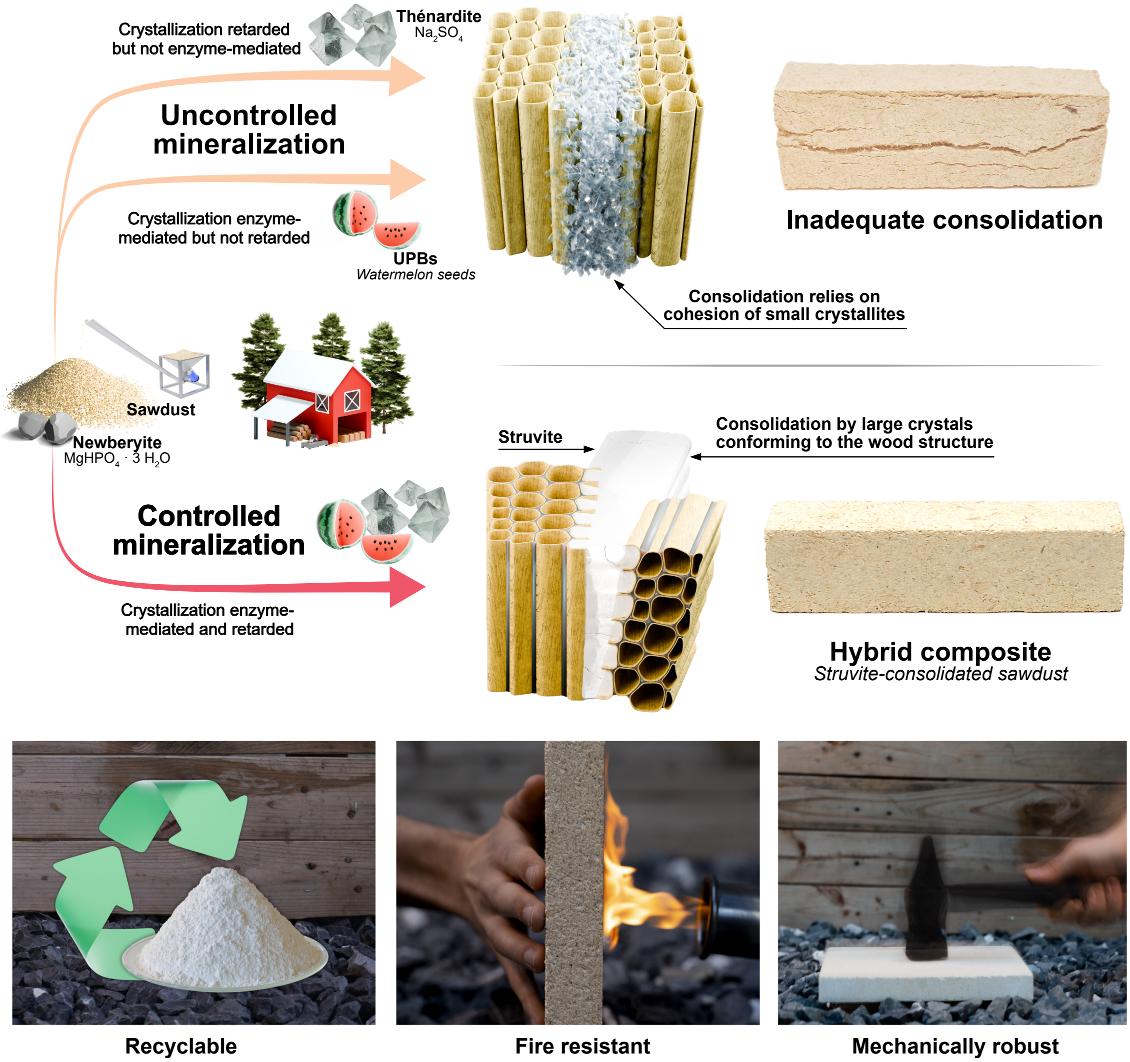

Figure 1. Sawdust consolidation by controlled enzyme-mediated struvite crystallization

The mineralization of struvite under confinement can be controlled by the urease-catalyzed hydrolysis of urea combined with the retardation of the crystallization by Na^+ and SO_4^{2-} ions, resulting in the formation of large struvite crystallites templated by sawdust. The resulting hybrid composites are recyclable, exhibit low propensity to either start or propagate a fire, and are mechanically robust.

that failed to effectively consolidate sawdust (Figures 1 and S1). This uncontrolled nucleation led to a dispersed mineral phase lacking the interparticle bridging necessary for the formation of strong composites. To achieve controlled struvite crystallization within the confined sawdust matrix, we implemented an enzymatic approach. This method uses the urease-catalyzed hydrolysis of urea to obtain a gradual release of ammonium ions and a controlled pH increase. UPBs extracted from watermelon seeds provided a stable, readily available source of urease.

Extraction of UPBs

Urease constitutes approximately 0.5 wt % of watermelon seeds,[24] alongside oil (∼50 wt %), other proteins (∼36 wt %), and fiber (∼5 wt %).[25] UPBs (membrane-lined organelles) were extracted from ground watermelon seeds with acetone, separated from husk residues, and dried, resulting in a free-flowing powder (Figure 2A). This powder was obtained with a yield of ∼25% and consisted of spherical particles up to ∼5 μm (Figure 2B). Isolated urease undergoes a drastic reduction in enzymatic activity as a result of the harsh conditions required for sawdust consolidation with struvite (high urea concentration, leading to substrate inhibition[26] and high ionic strength[27]). By contrast, UPBs maintain their enzymatic activity not only during material formation but also during prolonged storage under ambient conditions.[28] As such, they provide an ideal, stable source of urease for material synthesis.[29,30]

Enzymatic struvite precipitation

The enzymatic precipitation of struvite under the conditions used for the consolidation of sawdust—i.e., under confinement, at high precursor concentrations, and at room temperature

Please cite this article in press as: Kürsteiner et al., Enzyme-mediated consolidation of lignocellulosic materials with a flame-retardant and fully recyclable mineral binder, Chem Circularity (2025), https://doi.org/10.1016/j.checir.2025.100004

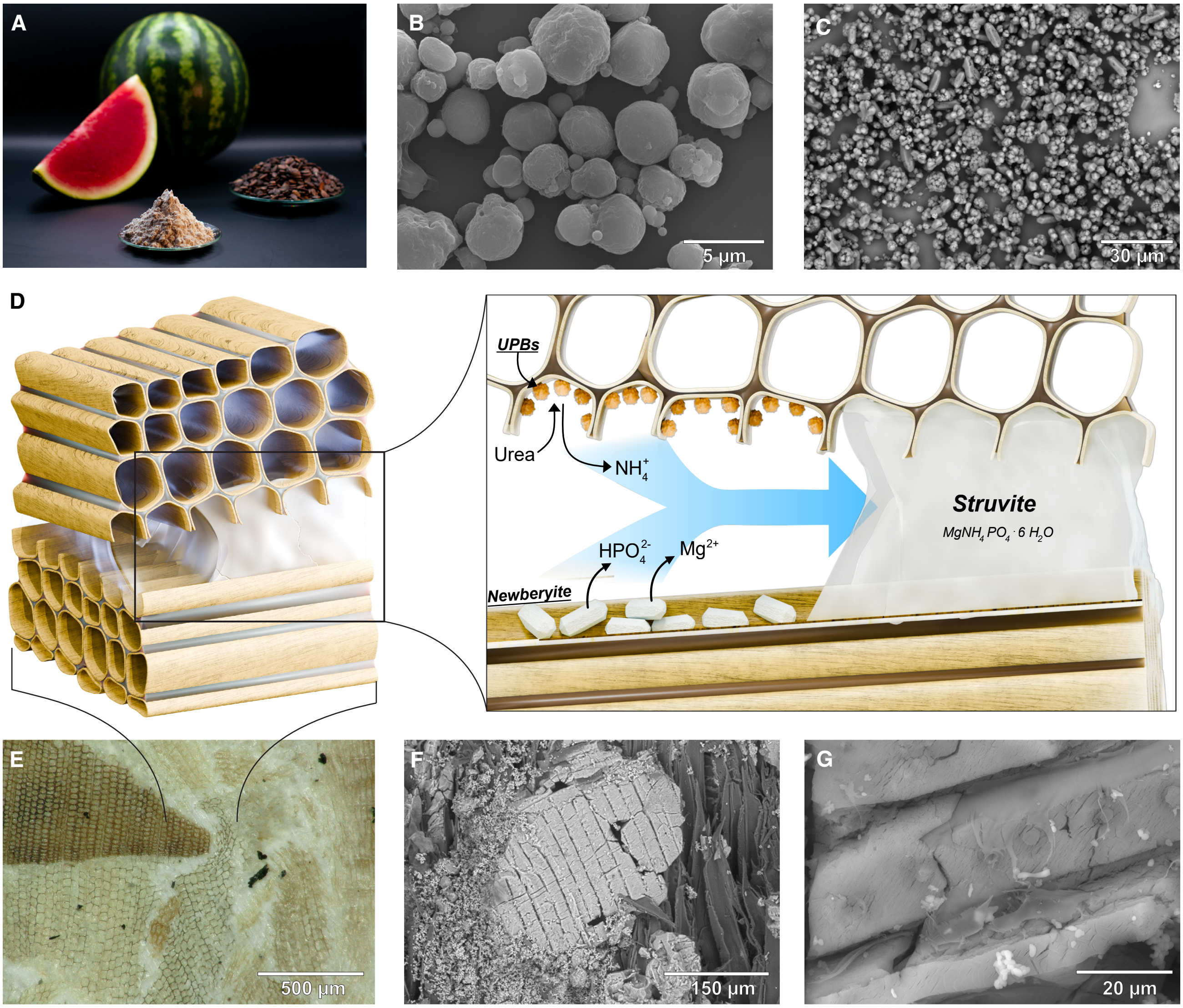

Figure 2. Synthesis of struvite-bonded sawdust composites

(A) Free-flowing powder of UPBs extracted from watermelon seeds.

(B) A secondary electron micrograph of UPBs shows spherical particles up to ~5 µm in size. Scale bar: 5 µm.

(C) Backscattered electron micrograph of the newberyite precursor with crystallite sizes < 10 µm. Scale bar: 30 µm.

(D) Schematic representation of the enzymatically induced SMPT from newberyite to struvite under confinement.

(E) Photomicrograph of the struvite-bonded sawdust composites. Scale bar: 500 µm.

(F) A backscattered electron micrograph of a fracture surface shows a large struvite crystal templated by a sawdust particle. Scale bar: 150 µm.

(G) Higher-magnification micrograph of a struvite crystal that displays templating by bordered pits of Norway spruce. Remnants of the cell wall indicate partial cohesive failure. The bright, small (<2 µm) particles represent Na_2SO_4 (thénardite). The fractured appearance of struvite crystals is due to their decomposition under imaging conditions (high vacuum and electron-beam irradiation) into mesoporous magnesium phosphate.[15] Scale bar: 20 µm.

(RT)—relies on a gradual dissolution of newberyite. In our system, the kinetics of struvite precipitation are primarily controlled by the NH_4^+ liberated by the enzymatic hydrolysis of urea and the dissolution rate of newberyite. We found that commercial newberyite contained large crystallites (up to ~200 µm), some of which remained in the final composite (Figure S2A). To facilitate newberyite dissolution, we synthesized a precursor suspension containing only small crystallites (<10 µm) (Figures 2C and S2B). As a result, only minor amounts of newberyite were left in the final composite (Figure S3A). During composite formation, the Mg^{2+} and HPO_4^{2-} ions from the dissolution of newberyite and the ammonia liberated from the enzymatic hydrolysis of urea by UPBs formed struvite in the newly established basic environment (Figure 2D). The crystallite size of struvite strongly depends on the presence of additional ions during crystallization. It is noteworthy that the presence of Na^+ and SO_4^{2-} ions retards the induction time of struvite precipitation.[31,32] Tests performed with various concentrations of Na_2SO_4 in the precursor

Please cite this article in press as: Kürsteiner et al., Enzyme-mediated consolidation of lignocellulosic materials with a flame-retardant and fully recyclable mineral binder, Chem Circularity (2025), https://doi.org/10.1016/j.checir.2025.100004

suspension showed that the crystallite size of struvite increased as the Na_2SO_4 concentration increased (Figures S2C–S2F). For the synthesis of the sawdust-struvite composites, we used an equimolar concentration of Na_2SO_4 ($[SO_4^{2-}] = [PO_4^{3-}]$) to balance the amount of soluble components remaining in the final composite while improving struvite crystallization.

Microstructure of the composites

In the formed composite, the mineral phase surrounded the sawdust particles (Figure 2E). Fracture surfaces of the composites revealed large struvite crystallites of several hundred micrometers, alongside small thénardite (Na_2SO_4) crystallites (Figure 2F). Interestingly, the controlled crystallization under confinement allowed the struvite crystals to conform to the substrate, effectively using the sawdust surface as a template. Moreover, this templating replicated not only large-scale features, such as cell walls and lumina, but also more delicate features, such as cell-wall openings (bordered pits) (Figure 2G). Analysis of fracture surfaces showed remnants of the cell wall adhering to the struvite crystallites, suggesting good adherence of the mineral phase to the wood substrate, which leads to partial cohesive failure. The sawing of wood leads to ruptured and torn cell walls, effectively increasing the surface area of the sawdust particles. When combined with a mineral binder able to conform to the topography of the substrate, this leads to strong mechanical interlocking.

As a result of the unidirectional compaction during composite formation, a preferential orientation of the highly anisotropic sawdust particles was evident. To investigate this preferential orientation as well as the distribution of the mineral phase, we performed microtomography on composites formed with either <4 or >4 mm sawdust fractions. The mineral phase was isolated from both the sawdust and the voids on the basis of their X-ray attenuation. As shown in Figures 3A and 3D, the mineral binder (blue) was homogeneously distributed throughout the composite regardless of the sawdust fraction used. Microtomography performed at higher resolution (Figure S4) revealed that the mineral phase encapsulates the sawdust particles and bridges between them. Although the lumina in the bulk of the sawdust particles were predominantly free of mineral binder, struvite did crystallize into accessible lumina at the surface of the sawdust particles, further increasing the mechanical interlocking (Figure S5). The composites showed a low porosity of ~2% (Figure S4G), which can be attributed to the small amount of water used for their preparation and the ability of sawdust to adsorb said water.

We define the long axis of the composites as the parallel direction, denoted as [||], and the short axis parallel to the direction of compaction as the perpendicular direction, denoted as [⊥]. Whereas directions are denoted with square brackets, planes are denoted with parentheses, i.e., planes normal to [⊥] are denoted as (⊥) (see Figures 3G and S4H). Analysis of the microtomography data showed that the sawdust particles aligned preferentially in (⊥) for composites formed with sawdust fractions < 4 mm (Figures 3B and 3C) and > 4 mm (Figures 3E and 3F). We determined the orientation of the sawdust particles in the composites as the direction of their major inertia axis. Figures 3H and 3I show the distribution of polar angles of sawdust particles with a volume > 2 mm^3 for the <4 and >4 mm sawdust fractions, respectively, where 90° corresponds to an alignment in (⊥), perpendicular to the direction of compaction. In both cases, the sawdust particles showed a strong tendency to preferentially orient during compaction; ~$^2/_3$ of the particles showed a polar angle > 75°. As will be shown in the following section, this preferred orientation markedly affected the mechanical properties of the composites.

Mechanical properties

The mechanical properties of the formed composites were tested in tension (as a measure of the wood-mineral interface), in compression, and in three-point bending. Three different sawdust fractions (<4 mm, >4 mm, and a 1:1 mixture thereof; Figures 4A and S3B) and the influence of packing density (low density: ~480 kg m^{-3}; high density: ~780 kg m^{-3}; Figure S3C) were investigated.

Tensile tests performed on high-density composites with a <4 mm sawdust fraction were conducted in [||] and [⊥]. As shown in Figure 4B, the transverse tensile strength in [⊥] was ~3.5 times lower than that in [||]. We attribute the comparatively low transverse tensile strength in [⊥] of 0.179 ± 0.015 MPa to failure of the wood-mineral interface under tension given that the sawdust particles were predominantly oriented in the fracture plane (Figure S6A). Conversely, the comparatively high transverse tensile strength in [||] of 0.673 ± 0.042 MPa can be attributed to the failure of the wood-mineral interface under shear given that the sawdust particles were predominantly oriented perpendicularly to the fracture plane (Figure S6A).

The mechanical properties of the composites strongly depend on their densities. The strength values of the high-density composites tend to be about three to four times higher than those of their low-density analogs, both under compression (Figure 4C) and under bending (Figure 4D), and are essentially independent of the sawdust fraction used. The strong dependence on density can be attributed to the larger void space for the low-density composites, which promotes the formation of large struvite crystallites that do not sufficiently bridge adjacent sawdust particles. Increasing the confinement leads to the formation of struvite crystallites that bridge sawdust particles, leading to effective consolidation. The mechanical performance of the composites was found to be largely independent of the size of the sawdust fraction, most likely because of a balance of opposing effects: smaller particles increase the interfacial area, potentially reducing stress concentrations at the wood-mineral interface, while larger particles might help arrest crack propagation through more effective deflection pathways.

Under compression in [||], the high-density composites reached a compressive strength ($\sigma_{C,||}$) of ~3 MPa, compared with a $\sigma_{C,\perp}$ of ~4.5 MPa in [⊥]. As for the tensile tests, this can be attributed to a different loading mode of the wood-mineral interface and hence drastically different failure modes. During compression in [||], a complex anisotropic stress state arose as a result of the preferential orientation of the sawdust particles in planes parallel to the load. The wood-mineral interface of particles oriented in (⊥) experienced not only loading under shear but also loading under tension as a result of a pronounced transverse deformation due to the Poisson effect, leading to failure in [⊥] (Figure S6B). Compression in [⊥] led to significantly different behavior given that the sawdust particles were aligned perpendicularly to the load and the composite underwent densification (Figure S6C), analogously

Please cite this article in press as: Kürsteiner et al., Enzyme-mediated consolidation of lignocellulosic materials with a flame-retardant and fully recyclable mineral binder, Chem Circularity (2025), https://doi.org/10.1016/j.checir.2025.100004

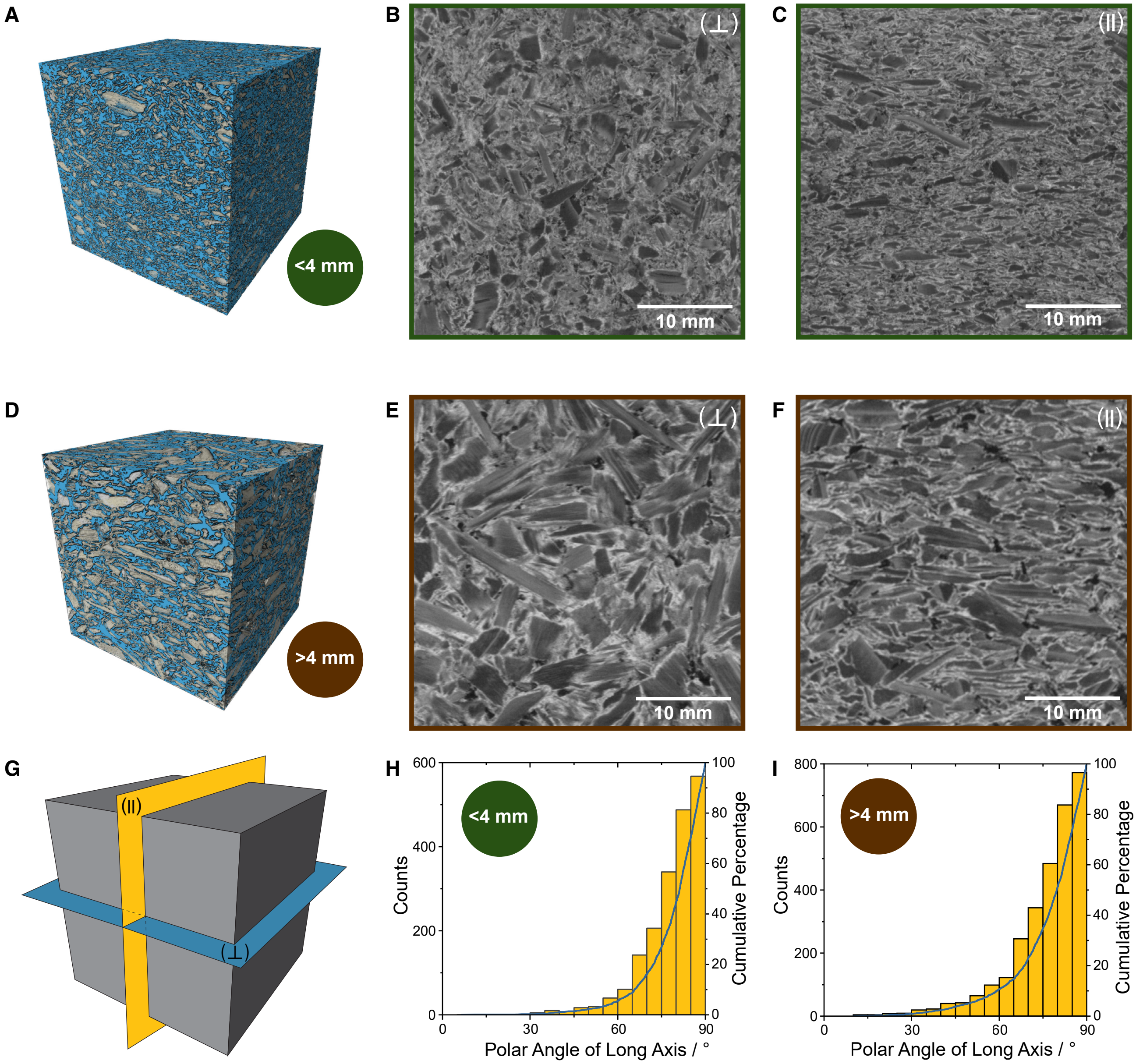

Figure 3. Microtomography of composites with a density of $\sim$780 kg m^{-3} ("high-density composites") for texture analysis

(A–C) Composite with <4 mm sawdust fraction.

(D–F) Composite with >4 mm sawdust fraction.

(A and D) 3D reconstruction (35 × 35 × 35 mm^3) of the microtomography data; the inorganics are colored in blue.

(B and E) The sawdust particles are randomly oriented in (⊥). Scale bars: 10 mm.

(C and F) In (||), the texture of the sawdust particles is visible. Scale bars: 10 mm.

(G) Schematic representation of the orientation of (A) and (B). (⊥) is shown in blue, and (||) is shown in yellow.

(H and I) Quantification of the texture present in the composites for <4 mm (H) and >4 mm (I) sawdust fractions. As a cutoff, a particle volume of 2 mm^3 was chosen in both instances. The particles are preferentially aligned in (⊥), and $\sim$2/3 of particles show a polar angle of the long axis of >75°, where 90° corresponds to alignment in (⊥).

See also Figure S4.

to native bulk wood compressed in the transverse directions. When loaded under compression in [⊥], the sawdust bricks exceeded the compressive strength of bulk Norway spruce in the transverse directions of $\sim$4.2 MPa.[33] As in other unidirectionally compressed chip-based composites, the moduli of elasticity in the two directions differed strongly[34] with an $E_{C,\parallel}$ of $\sim$300 MPa and an $E_{C,\perp}$ of $\sim$40 MPa (Figures 4E and 4F) for the high-density composites. For the low-density composites, the elastic moduli

Please cite this article in press as: Kürsteiner et al., Enzyme-mediated consolidation of lignocellulosic materials with a flame-retardant and fully recyclable mineral binder, Chem Circularity (2025), https://doi.org/10.1016/j.checir.2025.100004

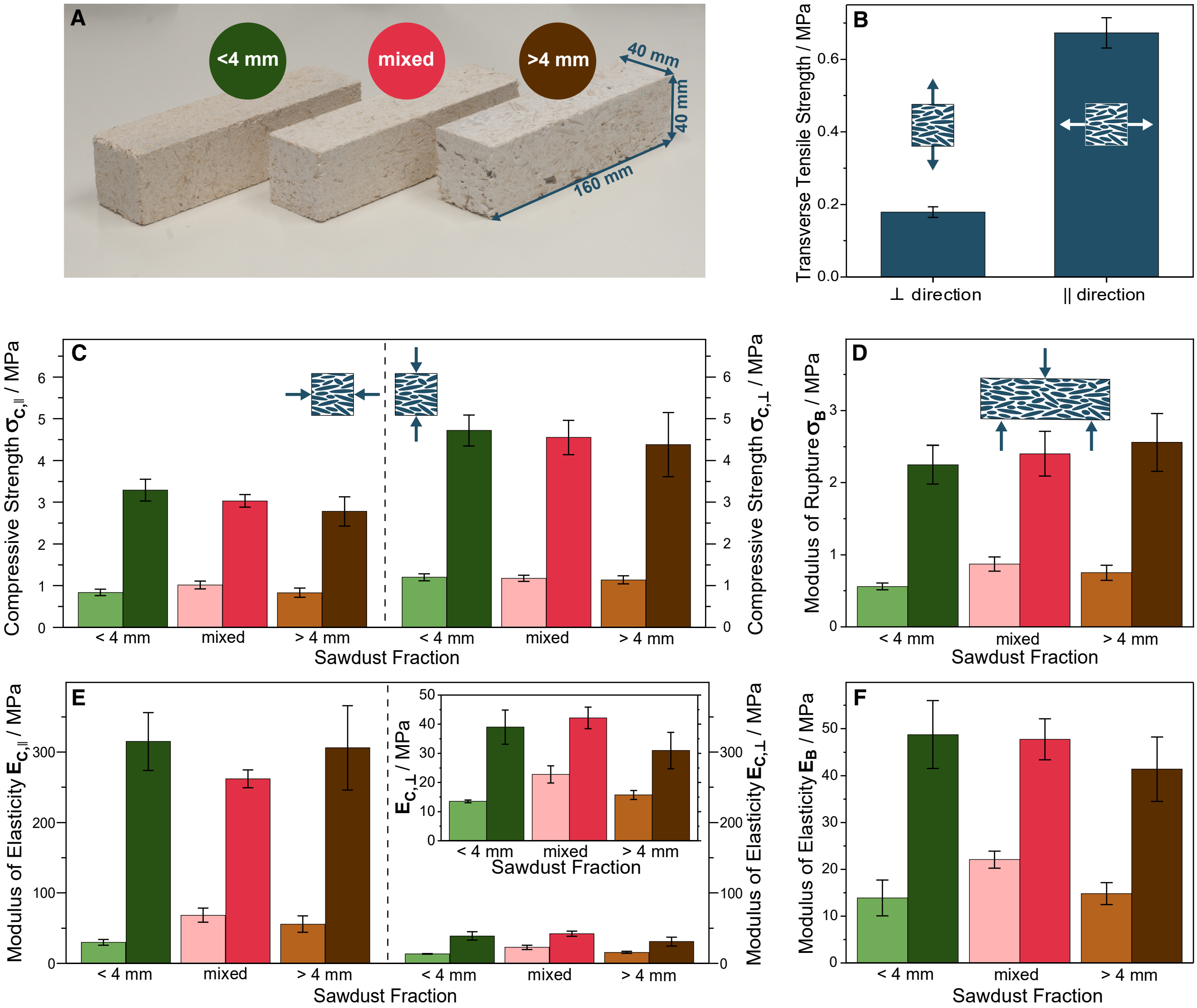

Figure 4. Mechanical properties of sawdust-struvite composites

(A) Struvite-bonded sawdust composites with <4 mm (left), mixed (middle), and >4 mm (right) sawdust fractions. The size of the specimens is 160 × 40 × 40 mm^3.

(B) The transverse tensile strength for the composite with <4 mm sawdust fraction in [⊥] was ~3.5× lower than in [||].

(C) Comparison of the compressive strengths for low-density (~480 kg m^{-3}; light green, pink, and light brown) and high-density (~780 kg m^{-3}; dark green, red, and dark brown) composites for the different sawdust fractions in [||] and [⊥]. The compressive strength depends predominantly on the density of the composites, and the difference between sawdust fractions is statistically insignificant.

(D) The trends seen during compression tests also apply to three-point bending tests.

(E) Elastic properties for the compression tests show strong anisotropy as a result of preferential particle alignment during unidirectional compaction.

(F) Comparison of the elastic moduli during the bending tests.

All values given are the mean of ten specimens; error bars denote one standard deviation.

for the mixed sawdust fraction exceeded those of the fractioned sawdust specimens in all tests conducted. This might be attributed to the more efficient space filling of multimodal particle-size distributions. In three-point bending, the high-density composites exhibited a modulus of rupture of ~2.4 MPa and a modulus of elasticity of ~45 MPa.

Flame-retardant properties

The flame-retardant performance of the prepared composites was investigated in terms of their reaction to fire (flammability and forced-combustion tests) and their resistance to fire (flame-penetration test).

Flammability tests evaluate samples' reactions to direct flame exposure (Figure 5A). When a flame is applied to either the edge or the surface of the composite, charring occurs within the area of contact (Figures 5B, 5C, S7A, and S7B). We observed no flame propagation either during flame application or upon its removal, thus indicating an overall non-igniting behavior where the majority of the sample remained undamaged (mass loss < 1%). This result suggests an extremely limited propensity

Please cite this article in press as: Kürsteiner et al., Enzyme-mediated consolidation of lignocellulosic materials with a flame-retardant and fully recyclable mineral binder, Chem Circularity (2025), https://doi.org/10.1016/j.checir.2025.100004

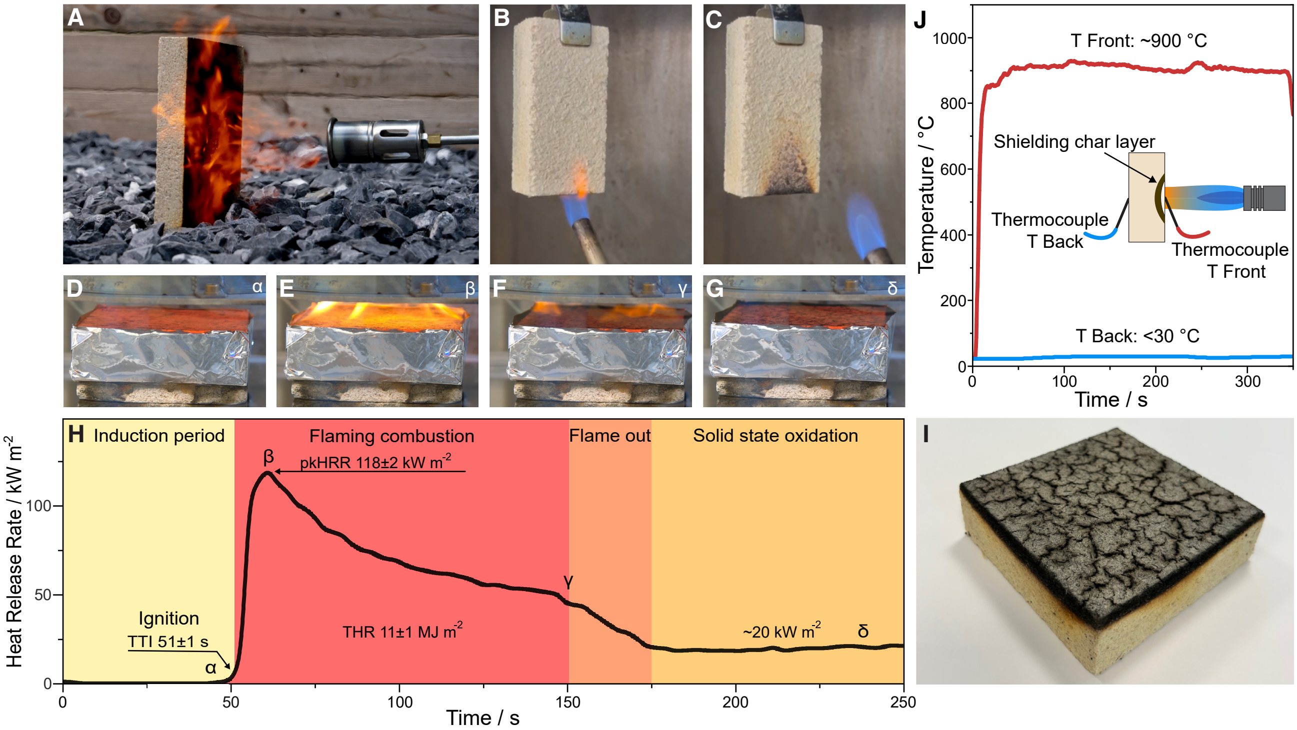

Figure 5. Flame-retardant properties of sawdust-struvite composites

(A) Struvite-bonded sawdust composite (200 × 200 × 30 mm^3) during exposure to a 50 kW flame after 30 s.

(B) Specimen at the beginning of the flammability test according to ISO 11925-2:2020.

(C) Specimen showing minimal surface charring after the flammability test.

(D–G) Specimen undergoing forced combustion under a heat flux of 50 kW m^{-2} during the induction period (D), after ignition (E), just before flameout (F), and during solid-state oxidation (G).

(H) Heat release rate (HRR) during forced combustion measurement.

(I) Residue showing a passivating char layer on the exposed surface after forced combustion.

(J) Temperature profiles during the flame-penetration test.

See also Figure S7.

of the prepared composite to start a fire. During forced-combustion tests (Figures 5D–5I), the sample was exposed to a 50 kW m^{-2} heat flux, simulating a fire in its early stage.[19] This triggered the release of flammable volatiles that, upon reaching the lower flammability limit, ignited and led to the flaming combustion of the sample. The prepared composite panels ignited after an average induction period (pre-ignition phase) of 51 ± 1 s (TTI) and reached a peak HRR (pkHRR) of 118 ± 2 kW m^{-2}. During combustion, extensive charring occurred on the surface of the samples, building up a barrier capable of both slowing down the release of volatiles from the sample and limiting heat transfer from the flame. This gradually reduced the HRR values until flameout occurred, signaling the end of active combustion. After flameout, a low HRR signal of ~20 kW m^{-2} remained as a result of the solid-state oxidation of the char in close proximity to the surface. As far as smoke is concerned, the prepared composites yielded an extremely low total smoke release (TSR) rate (Figure S7C) of 74 ± 4 $\text{m}^2\,\text{m}^{-2}$. Both the HRR and TSR rate represent important fire-hazard parameters in many application fields.[17,18] Therefore, the low heat and smoke-release values measured for the prepared composites confirm their excellent flame-retardant properties. After the test, the specimens showed a charred surface with nearly undamaged edges and backs, suggesting that only the upper portion of the sample and a small volume underneath the exposed surface were involved in the combustion. This was further supported by the high residual weight (88 ± 4 wt %). The fire resistance of the composites was also evaluated by means of a lab-scale flame-penetration test (Figure 5J). During this test, the surface of the sample was continuously exposed to a butane flame so that the surface reached ~900°C (Figure S7D). This promoted the formation of a thermally stable char layer that successfully insulated the back side of the sample (Figures S7E and S7F), where the temperature remained below 30°C for the entire duration of the test, i.e., over 5 min. The stability of the char layer was further confirmed by a high residual weight of 93 ± 1 wt %.

Although the performed forced-combustion tests are not directly comparable to the required calorimetric test for classification according to the Euroclass system (EN 13501), multivariate discriminant analysis on wood-based materials,[35] which aims to correlate cone calorimetry data to the Euroclass system, predicts that the presented material would most likely fall in Euroclass B. According to the performed flammability tests, which would also be conducted as part of the Euroclass classification, our material

Please cite this article in press as: Kürsteiner et al., Enzyme-mediated consolidation of lignocellulosic materials with a flame-retardant and fully recyclable mineral binder, Chem Circularity (2025), https://doi.org/10.1016/j.checir.2025.100004

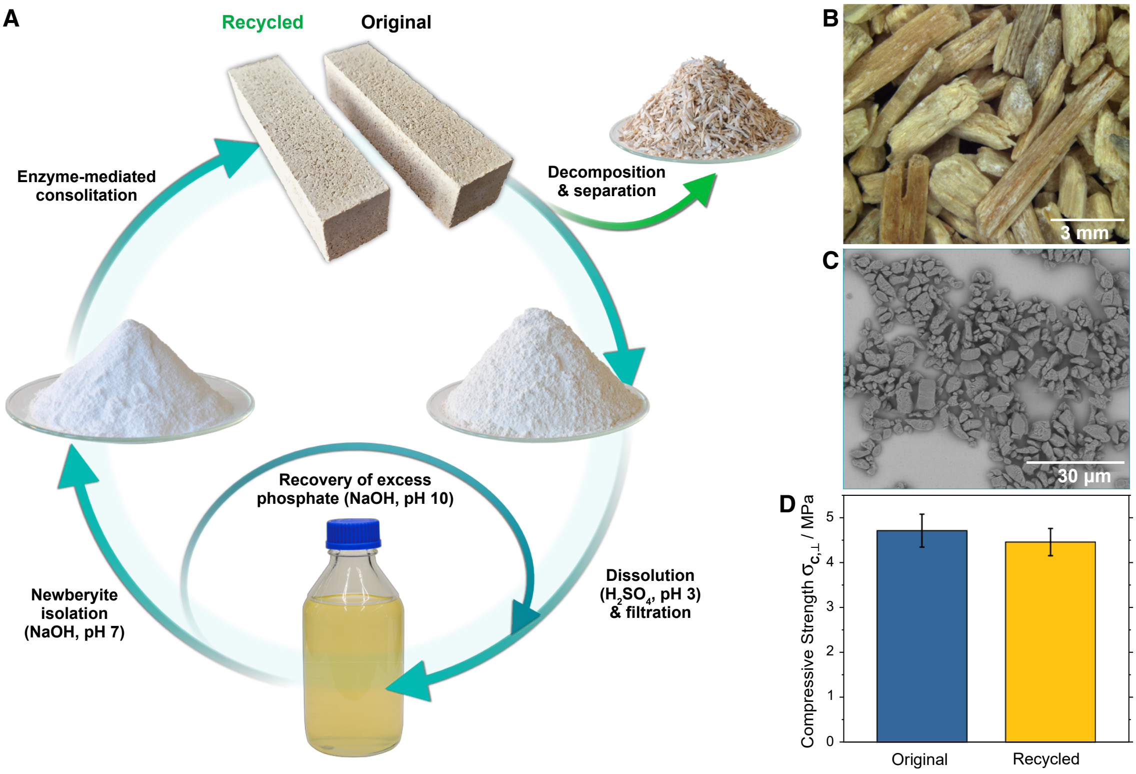

Figure 6. Recycling of the inorganic binder

(A) Recovery protocol of the newberyite precursor from spent composites.

(B) The inorganic binder can be effectively separated from the sawdust by mechanical means after thermal decomposition of struvite into amorphous magnesium phosphate. Scale bar: 3 mm.

(C) Precipitated newberyite from the recovered binder shows crystallite sizes < 10 µm. Scale bar: 30 µm.

(D) The mechanical properties of composites made from recycled newberyite show no statistically significant difference from those of the original composites. Values given are the mean of ten specimens; error bars denote one standard deviation.

See also Figure S8.

fulfills the requirements for a B rating. Indeed, from the flame-retardant characterization, it can be concluded that the prepared composites would not only have a limited propensity to either start or propagate a fire but also display a notable fire-shielding ability. Such behavior can be ascribed to the homogeneous distribution of struvite in the composite.

Recycling of the mineral binder

Because struvite can be used as a slow-release N/P fertilizer,[20,36] spent composites have the potential to be used for soil amendment or remediation by acting as a source of carbon, nitrogen, and phosphorus. However, the SMPT used for sawdust consolidation also allows for the mineral phase to be recycled under mild conditions. The recycling process involves the thermal decomposition and mechanical separation of struvite followed by dissolution using sulfuric acid and precipitation of newberyite via controlled pH titration (Figure 6A). We broke apart spent specimens from mechanical testing by using a disk mill and decomposed them at 103°C, forming amorphous magnesium phosphate[15] and leaving thénardite as the only crystalline inorganic phase (Figure S8E). This step is crucial because struvite preferentially precipitates over newberyite from equimolar concentrated solutions, and the large newberyite crystallites (>100 µm) formed by direct SMPT are unsuitable for sawdust consolidation.[22,37]

After thermal decomposition, we mechanically separated the inorganic phases from the sawdust (Figures 6B and S8A–S8D), dissolved the inorganic material in H_2SO_4, and removed the remaining wood fibers by filtration. We titrated the filtrate with NaOH to pH 7, precipitating newberyite crystallites of <10 µm (Figures 6C and S8F), which we used to form recycled composites. We collected the precipitated newberyite before quantitative phosphate recovery to avoid contamination with other phases. The remaining phosphate in solution was recovered and added to subsequent recycling runs. Recycled high-density composites with a <4 mm sawdust fraction exhibited a $\sigma_{C,\perp}$ of 4.45 ± 0.30 MPa, comparable to those of the original composites (4.71 ± 0.37 MPa; Figure 6D). The mild conditions used for newberyite recovery not only make the recycling of spent composites feasible but also facilitate the use of alternative struvite sources, such as precipitates from wastewater facilities, as a sustainable precursor for this process.[38–40]

Conclusion

This study demonstrates a green chemical approach for consolidating wood by-products, specifically sawdust, into

Please cite this article in press as: Kürsteiner et al., Enzyme-mediated consolidation of lignocellulosic materials with a flame-retardant and fully recyclable mineral binder, Chem Circularity (2025), https://doi.org/10.1016/j.checir.2025.100004

high-performance composites by using struvite as a mineral binder. An enzymatically induced SMPT from newberyite to struvite allowed controlled crystallization under confinement. The gradual release of ammonium ions via the urease-catalyzed hydrolysis of urea, with UPBs extracted from watermelon seeds, proved crucial for achieving large, well-defined struvite crystals that intimately template the sawdust surface. This templating, extending to microscopic anatomical features, resulted in exceptional mechanical interlocking and thus strong composites at a low binder-to-sawdust ratio. The observed anisotropy in mechanical properties results from the preferential orientation of sawdust particles induced during unidirectional compaction. Indeed, microtomography confirmed the presence of a strong preferential particle orientation perpendicular to the direction of compaction. The homogeneous distribution of the mineral phase and its ability to conform to the complex topography of sawdust particles contribute to the enhanced mechanical and flame-retardant performance.

The demonstrated recyclability of the struvite binder represents a significant advancement toward the implementation of circular economy principles for building materials. The ability to recover and reuse struvite and the potential to upcycle struvite precipitates from wastewater facilities further emphasize the sustainability of this approach. The recycled composites exhibit mechanical strength comparable to that of the originals. Thus, our sawdust-struvite composites offer a viable, eco-friendly choice for applications in the building sector, which requires highly flame-retardant materials.

METHODS

Materials and chemicals

Watermelon seeds (*Citrullus lanatus*) of the variety "Crimson Sweet" were obtained from RB Sementi. Softwood sawdust was obtained from a local sawmill (Blumer Lehmann) and conditioned at 20°C and 65% RH (moisture content of ~12%). The sawdust consisted primarily of Norway spruce (*Picea abies*) but could have contained other native softwood species, such as European silver fir (*Abies alba*) and pine (*Pinus* spp.). The sawdust was fractioned with a 4 mm analytical sieve. Di-basic sodium phosphate dihydrate ($Na_2HPO_4 \cdot 2H_2O$, AnalaR NORMAPUR), urea (ACS reagent, 99.0%–100.5%), and sulfuric acid (H_2SO_4, 95%) were purchased from VWR Chemicals. Magnesium sulfate ($MgSO_4$, $\geq$99.5%), ammonium carbonate ($(NH_4)_2CO_3$, ACS reagent, $\geq$30% NH_3 basis), sodium sulfate (Na_2SO_4, ACS reagent, $\geq$99.0%), sodium hydroxide (NaOH, ACS reagent, $\geq$98.0%), and acetone (ACS reagent, $\geq$99.5%) were purchased from Sigma-Aldrich.

Extraction of UPBs

Watermelon seeds were ground with a high-speed grinder (25,000 rpm). Stirring the ground material in acetone for 1 h released the protein bodies, which were separated from shell particles with a 125 μm sieve and collected via vacuum filtration. The UPBs were stirred in acetone overnight, collected via vacuum filtration, and dried in a vacuum desiccator at RT, ensuring homogeneous distribution in the composite. The acetone was recovered via vacuum distillation and used for subsequent extractions.

Preparation of precursor suspension

$Na_2HPO_4 \cdot 2H_2O$ was dissolved in H_2O (105 mL per specimen) under gentle heating to ~40°C. Under vigorous stirring in a planetary mixer, 1 equiv of $MgSO_4$ was added and stirred for 1 h at ~40°C. (The exothermic addition of $MgSO_4$ can lead to the formation of a stiff gel if not stirred sufficiently.) The formation of a gel did not negatively affect the crystallite size of the newly formed newberyite, and a suspension could still be obtained via sufficient stirring after gelation. Finally, 1.25 equiv urea was added and stirred for 15 min. The precursor concentrations were chosen such that $m_{struvite}/m_{sawdust} = 0.65$ (2.65 $mmol_{struvite}$ $g^{-1}_{sawdust}$).

For the preparation of composites with varying amounts of Na_2SO_4, the newberyite precursor (prior to the addition of urea) was washed twice with H_2O, isolated by vacuum filtration, and dried under vacuum at RT.

For the preparation of composites with varying amounts of Na_2SO_4 (0, 0.1, 0.5, and 1 equiv), commercial newberyite (1 equiv Na_2SO_4), or reclaimed newberyite (1 equiv Na_2SO_4), the newberyite powder was suspended in H_2O and stirred with Na_2SO_4 at 40°C for 1 h prior to the addition of urea.

Preparation of composites

65 and 105 g sawdust was mixed with 370 and 600 mg UPBs, respectively, for the low- and high-density composites, respectively. To this, the precursor suspension was added and mixed until a homogeneous mixture was obtained. The sawdust mixture was added to the mold and compacted to $160 \times 40 \times 40$ mm^3 (~2 MPa for the high-density composite). The specimens were demolded after 48 h and conditioned at 20°C ± 2°C and 65% ± 5% RH until the mass loss over a 24 h period was less than 0.1%. For flammability, forced-combustion, and flame-penetration tests, $230 \times 230 \times 30$ mm^3 plates were prepared accordingly and cut to size with a circular saw (Figure S3D).

Recovery of newberyite precursor

Spent specimens from mechanical testing were broken apart in a disk mill (FRITSCH Pulverisette 13) and decomposed at 103°C for 1 day in a ventilated convection oven. Separation of the inorganic material was performed in a vibratory sieving tower (FRITSCH Analysette). After an initial separation step, the >125 μm fractions were passed through the disk mill again and sieved. The <125 μm fraction was decomposed for another day at 103°C until the complete decomposition of struvite. A 25 wt % suspension in H_2O was dissolved by the addition of H_2SO_4 to pH 3 and filtered through Celite Hyflo Super Cel with a ROBU porosity 4 sintered glass frit for the removal of residual wood fibers. The filtrate was titrated to pH 5 with 2 M NaOH, and stirring for 30 min induced nucleation. The suspension was then gradually titrated to pH 7 via the addition of 0.2 M NaOH and stirred for another 15 min. Finally, the newberyite precursor was collected by vacuum filtration, washed, and dried at RT. The remaining phosphate in the filtrate was precipitated by titration to pH 10, collected by vacuum filtration, dried, and added to subsequent recycling runs.

Characterization

Three-point bending tests were performed on a Zwick Roell Z010 universal testing machine using a 100 mm support span

Please cite this article in press as: Kürsteiner et al., Enzyme-mediated consolidation of lignocellulosic materials with a flame-retardant and fully recyclable mineral binder, Chem Circularity (2025), https://doi.org/10.1016/j.checir.2025.100004

length and a constant rate of 1 mm min^{-1} on 40 × 40 × 160 mm^3 specimens. Compression tests were performed on a Zwick Roell Z010 or Z100 universal testing machine on 40 × 40 × 40 mm^3 specimens at a constant rate of 1.5 mm min^{-1}. The modulus of elasticity and compressive strength were evaluated according to EN 408. Perpendicular tensile tests were performed on 40 × 40 × 40 mm^3 specimens mounted with high-viscosity epoxy resin on hardwood-plywood yokes at a constant rate of 0.5 mm min^{-1} on the basis of EN 319. For all mechanical tests, the values given are the mean of ten specimens, and error bars denote one standard deviation. All specimens were conditioned at 20°C ± 2°C and 65% ± 5% RH until the relative mass loss over a 24 h period was less than 0.1%.

Scanning electron microscopy was performed on a Hitachi SU5000. Energy-dispersive X-ray spectroscopy (EDS) was performed with two large-area window (100 mm^2) Oxford Ultim Max 100 EDS detectors. Optical microscopy was performed on a Keyence VHX 6000 digital light microscope.

X-ray diffraction was performed on a PANalytical X'Pert PRO MPD diffractometer in Bragg-Brentano geometry with monochromatic Cu $K_{\alpha 1}$ radiation (40 kV, 45 mA, germanium monochromator). The diffractograms were obtained with a step size of 0.0167° and a scan speed of 0.00833° s^{-1} under continuous spinning at 15 min^{-1} with an X-ray footprint of 10 × 10 mm^2. Analyses were performed with HighScore Plus.[41] The corresponding Inorganic Crystal Structure Database (ICSD)[42] collection codes are ICSD-750 for struvite,[43] ICSD-8228 for newberyite,[44] and ICSD-2895 for thénardite.[45]

The X-ray microtomographic studies were conducted with an EasyTom XL Ultra 230-160 micro/nano-CT scanner (RX Solutions). Micro-computed tomography (CT) analysis was performed on two different specimen sizes: 40 × 40 × 160 mm^3 for texture analysis and 10 × 10 × 20 mm^3 for high-resolution imaging. The operating voltage and current of the scanner were set to 70 kV and 120 μA, respectively. The samples underwent a full 360° continuous rotation with a total of 1,440 projections, a frame averaging of 10, and a frame rate of 6.00. The nominal resolution was set to either a 35 or 12 μm voxel size, depending on the size of the sample, to ensure increasingly higher resolution for the analysis of the sawdust particles. All CT datasets were reconstructed with the filtered back-projection algorithm with a small ring artifact reduction and an 80% Hann window function on RXAct software (RX Solutions). The reconstructed datasets were then resliced with the open-source image-processing software Fiji[46] so the sample volume could be examined from various angles and orientations. The generated CT datasets were processed and analyzed with Fiji[46] and the software application Avizo (Thermo Fisher Scientific). We calculated the mineral, sawdust, and porosity volume fraction of the samples, along with their distribution, by applying a global threshold to the tomographic cross-sections and determining the proportion of the single features relative to the total volume of the sample. The orientation of each sawdust particle was calculated with Avizo. Specifically, the orientation was determined in the transverse plane (represented as φ°) and relative to the longitudinal axis (θ°) of both the major and minor inertia axes of each single 3D particle. Specifically, the orientation analysis was based on the calculation of the covariance matrix and moments of inertia. This matrix provides the eigenvectors and eigenvalues necessary for orientation determination. The eigenvector corresponding to the largest eigenvalue defines the direction of the major inertia axis, whereas the eigenvector corresponding to the smallest eigenvalue defines the direction of the minor inertia axis.

The reaction to direct flame application was tested by flammability tests following the ISO 11925-2:2020 standard for what concerns flame characteristics (time, size, and orientation) and sample exposure to flame (edge and surface). During the test, a blue methane flame (2 cm) was applied for 30 s with the burner tilted at 45° to either the bottom edge or surface of specimens with dimensions of 100 × 50 × 30 mm^3. The behavior of the samples during flame application and upon flame removal and the final residue at the end of the tests were evaluated. Forced-combustion tests were performed on a cone calorimeter (Noselab-ATS) according to the ISO 5660 standard. Square samples (100 × 100 × 30 mm^3) were exposed in horizontal configuration to a 50 kW m^{-2} heat flux. During the test, the TTI (s), the average HRR (aHRR; kW m^{-2}) and its peak (pkHRR, kW m^{-2}), the total heat release (THR; MJ m^{-2}), the TSR (m^2 m^{-2}), and the final residue (wt %) were evaluated. Flame-penetration tests were performed for assessing the resistance of the composites to penetration of a 150 W flame generated from a butane flame torch according to a previously developed setup.[47] A square specimen (100 × 100 × 30 mm^3) was positioned in a metallic frame, leaving an exposed area of 80 × 80 mm^2, and held in a vertical configuration. A flame torch, positioned at a 50 mm distance from the surface of the specimen, was then applied continuously for 5 min. During the test, the temperature profiles on the exposed front side surface and on the unexposed back side of the specimen were measured by two thermocouples (stainless-steel sheathed K-type, 1 mm diameter). The two thermocouples were fixed in contact with the sample to prevent displacement during the test. The average temperature profiles were calculated from two specimens. Before flammability, cone-calorimetry, and flame-penetration tests, the test specimens previously conditioned at 20°C and 65% RH were conditioned in a climatic chamber at 23°C and 50% RH for 48 h.

RESOURCE AVAILABILITY

Lead contact

Requests for further information and resources should be directed to and will be fulfilled by the lead contact, Ronny Kürsteiner (ronnyk@ethz.ch).

Materials availability

This study did not generate new unique reagents.

Data and code availability

- All data reported in this paper will be shared by the lead contact upon request.
- This paper does not report original code.
- Any additional information required for reanalyzing the data reported in this paper is available from the lead contact upon request.

ACKNOWLEDGMENTS

R.K. and I.B. are part of SPEED2ZERO, a joint initiative co-financed by the ETH Board. G.P. expresses personal gratitude to Prof. John Pojman (Louisiana

State University) for sharing his knowledge (and a sample) of watermelon-seed UPBs. The authors gratefully acknowledge Dr. Thomas Weber from the D-MATL X-ray service platform at ETH Zurich for his support and assistance with X-ray characterization. The authors thank Blumer Lehmann AG (Gossau, Switzerland) for providing the sawdust particles and the Scientific Center for Optical and Electron Microscopy (ScopeM) of ETH Zurich for providing the electron microscopy facilities.

AUTHOR CONTRIBUTIONS

Writing – original draft, R.K.; writing – review & editing, R.K., D.V.G., M.R., A.P., J.G., L.M., C.H.D., F.C., I.B., and G.P.; investigation, R.K., D.V.G., M.R., A.P., L.M., T.S., C.H.D., and F.C.; formal analysis, R.K., D.V.G., A.P., L.M., and F.C.; visualization, R.K., D.V.G., M.R., and J.G.; methodology, R.K., D.V.G., and T.S.; conceptualization, R.K., I.B., and G.P.; funding acquisition, I.B.; supervision, I.B. and G.P.

DECLARATION OF INTERESTS

The authors declare no competing interests.

SUPPLEMENTAL INFORMATION

Supplemental information can be found online at https://doi.org/10.1016/j.checir.2025.100004.

Received: September 25, 2025
Revised: November 14, 2025
Accepted: December 29, 2025

REFERENCES

1. Zbieć, M., Franc-Dąbrowska, J., and Drejerska, N. (2022). Wood waste management in Europe through the lens of the circular bioeconomy. Energies *15*, 4352. https://doi.org/10.3390/en15124352.
2. Charis, G., Danha, G., and Muzenda, E. (2019). A review of timber waste utilization: Challenges and opportunities in Zimbabwe. Procedia Manuf. *35*, 419–429. https://doi.org/10.1016/j.promfg.2019.07.005.
3. Pandey, S. (2022). Wood waste utilization and associated product development from under-utilized low-quality wood and its prospects in Nepal. SN Appl. Sci. *4*, 168. https://doi.org/10.1007/s42452-022-05061-5.
4. Barlaz, M.A. (2006). Forest products decomposition in municipal solid waste landfills. Waste Manag. *26*, 321–333. https://doi.org/10.1016/j.wasman.2005.11.002.
5. Roy, P., Mohanty, A.K., and Misra, M. (2022). Microplastics in ecosystems: Their implications and mitigation pathways. Environ. Sci. Adv. *1*, 9–29. https://doi.org/10.1039/D1VA00012H.
6. de Souza Machado, A.A., Kloas, W., Zarfl, C., Hempel, S., and Rillig, M.C. (2018). Microplastics as an emerging threat to terrestrial ecosystems. Glob. Change Biol. *24*, 1405–1416. https://doi.org/10.1111/gcb.14020.
7. Albert, C.M., and Liew, K.C. (2024). Recent development and challenges in enhancing fire performance on wood and wood-based composites: A 10-year review from 2012 to 2021. J. Bioresour. Bioprod. *9*, 27–42. https://doi.org/10.1016/j.jobab.2023.10.004.
8. Wang, L., Chen, S.S., Tsang, D.C.W., Poon, C.-S., and Shih, K. (2016). Recycling contaminated wood into eco-friendly particleboard using green cement and carbon dioxide curing. J. Clean. Prod. *137*, 861–870. https://doi.org/10.1016/j.jclepro.2016.07.180.
9. Giancaspro, J., Papakonstantinou, C., and Balaguru, P. (2008). Fire resistance of inorganic sawdust biocomposite. Compos. Sci. Technol. *68*, 1895–1902. https://doi.org/10.1016/j.compscitech.2008.01.002.
10. Pan, F., Jia, H., Huang, Y., Chen, Z., Liang, S., and Jiang, P. (2023). Analyzing temperature distribution patterns on the facing and backside surface: Investigating combustion performance of flame-retardant particle boards using aluminum hypophosphite, intumescent, and magnesium hydroxide flame retardants. Polymers *15*, 4479. https://doi.org/10.3390/polym15234479.
11. Zhang, B., Duan, G., Qin, Q., Li, S., Zhou, W., Zhang, C., and Jiang, S. (2025). Advanced wood–inorganic composites: Preparation, properties and perspectives. Mater. Horiz. *12*, 2503–2523. https://doi.org/10.1039/D4MH01475H.
12. Ellis, L.D., Badel, A.F., Chiang, M.L., Park, R.J.-Y., and Chiang, Y.-M. (2020). Toward electrochemical synthesis of cement—An electrolyzer-based process for decarbonating $CaCO_3$ while producing useful gas streams. Proc. Natl. Acad. Sci. USA *117*, 12584–12591. https://doi.org/10.1073/pnas.1821673116.
13. Guo, H., Luković, M., Mendoza, M., Schlepütz, C.M., Griffa, M., Xu, B., Gaan, S., Herrmann, H., and Burgert, I. (2019). Bioinspired struvite mineralization for fire-resistant wood. ACS Appl. Mater. Interfaces *11*, 5427–5434. https://doi.org/10.1021/acsami.8b19967.
14. Guo, H., Özparpucu, M., Windeisen-Holzhauser, E., Schlepütz, C.M., Quadranti, E., Gaan, S., Dreimol, C., and Burgert, I. (2020). Struvite mineralized wood as sustainable building material: Mechanical and combustion behavior. ACS Sustain. Chem. Eng. *8*, 10402–10412. https://doi.org/10.1021/acssuschemeng.0c01769.
15. Hövelmann, J., Stawski, T.M., Besselink, R., Freeman, H.M., Dietmann, K. M., Mayanna, S., Pauw, B.R., and Benning, L.G. (2019). A template-free and low temperature method for the synthesis of mesoporous magnesium phosphate with uniform pore structure and high surface area. Nanoscale *11*, 6939–6951. https://doi.org/10.1039/C8NR09205B.
16. Bhuiyan, M.I.H., Mavinic, D.S., and Koch, F.A. (2008). Thermal decomposition of struvite and its phase transition. Chemosphere *70*, 1347–1356. https://doi.org/10.1016/j.chemosphere.2007.09.056.
17. Babrauskas, V., and Peacock, R.D. (1992). Heat release rate: The single most important variable in fire hazard. Fire Saf. J. *18*, 255–272. https://doi.org/10.1016/0379-7112(92)90019-9.
18. Fridolf, K., Andrée, K., Nilsson, D., and Frantzich, H. (2014). The impact of smoke on walking speed. Fire Mater. *38*, 744–759. https://doi.org/10.1002/fam.2217.
19. Schartel, B., and Hull, T.R. (2007). Development of fire-retarded materials—Interpretation of cone calorimeter data. Fire Mater. *31*, 327–354. https://doi.org/10.1002/fam.949.
20. Valle, S.F., Giroto, A.S., Dombinov, V., Robles-Aguilar, A.A., Jablonowski, N.D., and Ribeiro, C. (2022). Struvite-based composites for slow-release fertilization: A case study in sand. Sci. Rep. *12*, 14176. https://doi.org/10.1038/s41598-022-18214-8.
21. Yu, X., Yang, H., and Wang, H. (2022). A cleaner biocementation method of soil via microbially induced struvite precipitation: A experimental and numerical analysis. J. Environ. Manag. *316*, 115280. https://doi.org/10.1016/j.jenvman.2022.115280.
22. Abbona, F., Lundager Madsen, H.E., and Boistelle, R. (1982). Crystallization of two magnesium phosphates, struvite and newberyite: Effect of pH and concentration. J. Cryst. Growth *57*, 6–14. https://doi.org/10.1016/0022-0248(82)90242-1.
23. Cardew, P.T., Davey, R.J., and Birchall, J.D. (1985). The kinetics of solvent-mediated phase transformations. Proc. R. Soc. Lond. A Math. Phys. Sci. *398*, 415–428. https://doi.org/10.1098/rspa.1985.0043.
24. Mohamed, T., Mohamed, M.A., Mohamed, S.A., and Fahmy, A.S. (1999). Purification of urease from water melon seeds for clinical diagnostic kits. Bioresour. Technol. *68*, 215–223. https://doi.org/10.1016/S0960-8524(99)00157-1.
25. El-Adawy, T.A., and Taha, K.M. (2001). Characteristics and composition of watermelon, pumpkin, and paprika seed oils and flours. J. Agric. Food Chem. *49*, 1253–1259. https://doi.org/10.1021/jf001117%2B.
26. Deasy, C.L. (1947). The mechanism of urease inhibition by urea. J. Am. Chem. Soc. *69*, 294–295. https://doi.org/10.1021/ja01194a039.

Please cite this article in press as: Kürsteiner et al., Enzyme-mediated consolidation of lignocellulosic materials with a flame-retardant and fully recyclable mineral binder, Chem Circularity (2025), https://doi.org/10.1016/j.checir.2025.100004

27. Desmidt, E., Ghyselbrecht, K., Monballiu, A., Rabaey, K., Verstraete, W., and Meesschaert, B.D. (2013). Factors influencing urease driven struvite precipitation. Separ. Purif. Technol. *110*, 150–157. https://doi.org/10.1016/j.seppur.2013.03.010.
28. Mai, A.Q.Q. (2021). Characterization, immobilization, and polymer related applications of watermelon seed powder, a practical source of urease enzymeDoctoral dissertation (Louisiana State University). https://doi.org/10.31390/gradschool_dissertations.5464.
29. Mai, A.Q., Bánsági, T., Taylor, A.F., and Pojman, J.A. (2021). Reaction-diffusion hydrogels from urease enzyme particles for patterned coatings. Commun. Chem. *4*, 101. https://doi.org/10.1038/s42004-021-00538-7.
30. Markovic, V.M., Bánsági, T., Jr, McKenzie, D., Mai, A., Pojman, J.A., and Taylor, A.F. (2019). Influence of reaction-induced convection on quorum sensing in enzyme-loaded agarose beads. Chaos *29*, 033130. https://doi.org/10.1063/1.5089295.
31. Kabdaşlı, I., Atalay, Z., and Tünay, O. (2017). Effect of solution composition on struvite crystallization. J. Chem. Technol. Biotechnol. *92*, 2921–2928. https://doi.org/10.1002/jctb.5310.
32. Wu, J., Li, Y., Xu, B., Li, M., Wang, J., Shao, Y., Chen, F., Sun, M., and Liu, B. (2022). Effects of physicochemical parameters on struvite crystallization based on kinetics. Int. J. Environ. Res. Publ. Health *19*, 7204. https://doi.org/10.3390/ijerph19127204.
33. Niemz, P., and Sonderegger, W. (2017). Festigkeitseigenschaften. In Holzphysik: Physik des Holzes und der Holzwerkstoffe (Carl Hanser Verlag GmbH & Co. KG), pp. 336–414. https://doi.org/10.3139/9783446445468.014.
34. Wilczyński, A., and Kociszewski, M. (2012). Elastic properties of the layers of three-layer particleboards. Eur. J. Wood Prod. *70*, 357–359. https://doi.org/10.1007/s00107-010-0497-8.
35. Steen-Hansen, A., and Kristoffersen, B. (2007). Prediction of fire classification for wood based products. A multivariate statistical approach based on the cone calorimeter. Fire Mater. *31*, 207–223. https://doi.org/10.1002/fam.934.
36. Talboys, P.J., Heppell, J., Roose, T., Healey, J.R., Jones, D.L., and Withers, P.J.A. (2016). Struvite: A slow-release fertiliser for sustainable phosphorus management? Plant Soil *401*, 109–123. https://doi.org/10.1007/s11104-015-2747-3.
37. Boistelle, R., Abbona, F., and Lundager Madsen, H.E. (1983). On the transformation of struvite into newberyite in aqueous systems. Phys. Chem. Miner. *9*, 216–222. https://doi.org/10.1007/BF00311958.
38. Kecskésová, S., Imreová, Z., Martonka, M., and Drtil, M. (2020). Chemical dissolution of struvite precipitates in pipes from anaerobic sludge digestion. Chem. Pap. *74*, 2545–2552. https://doi.org/10.1007/s11696-020-01096-3.
39. Chandrasekaran, S., Zaffar, A., and Balasubramanian, P. (2024). Struvite in circular economy: Production techniques, emerging applications and market opportunities. WIREs Energy and Environment *13*, e529. https://doi.org/10.1002/wene.529.
40. Siciliano, A., Limonti, C., Curcio, G.M., and Molinari, R. (2020). Advances in struvite precipitation technologies for nutrients removal and recovery from aqueous waste and wastewater. Sustainability *12*, 7538. https://doi.org/10.3390/su12187538.
41. Degen, T., Sadki, M., Bron, E., König, U., and Nénert, G. (2014). The HighScore suite. Powder Diffr. *29*, S13–S18. https://doi.org/10.1017/S0885715614000840.
42. Zagorac, D., Müller, H., Ruehl, S., Zagorac, J., and Rehme, S. (2019). Recent developments in the Inorganic Crystal Structure Database: Theoretical crystal structure data and related features. J. Appl. Crystallogr. *52*, 918–925. https://doi.org/10.1107/S160057671900997X.
43. Fugel, M., Malaspina, L.A., Pal, R., Thomas, S.P., Shi, M.W., Spackman, M.A., Sugimoto, K., and Grabowsky, S. (2019). Revisiting a historical concept by using quantum crystallography: Are phosphate, sulfate and perchlorate anions hypervalent? Chem. Eur. J. *25*, 6523–6532. https://doi.org/10.1002/chem.201806247.
44. Abbona, F., Boistelle, R., and Haser, R. (1979). Hydrogen bonding in $MgHPO_4{\cdot}3H_2O$ (newberyite). Acta Crystallogr. B Struct. Sci. *35*, 2514–2518. https://doi.org/10.1107/S0567740879009791.
45. Nord, A.G., Sværen, S.E., Møller, J., Schroll, G., Leander, K., and Swahn, C.G. (1973). Refinement of the crystal structure of thenardite, Na_2SO_4. Acta Chem. Scand. *27*, 814–822. https://doi.org/10.3891/acta.chem.scand.27-0814.
46. Schindelin, J., Arganda-Carreras, I., Frise, E., Kaynig, V., Longair, M., Pietzsch, T., Preibisch, S., Rueden, C., Saalfeld, S., Schmid, B., et al. (2012). Fiji: An open-source platform for biological-image analysis. Nat. Methods *9*, 676–682. https://doi.org/10.1038/nmeth.2019.
47. Carosio, F., Medina, L., Kochumalayil, J., and Berglund, L.A. (2021). Green and fire resistant nanocellulose/hemicellulose/clay foams. Adv. Mater. Interfac. *8*, 2101111. https://doi.org/10.1002/admi.202101111.

CHECIR, Volume *1*

Supplemental information

Enzyme-mediated consolidation of lignocellulosic materials with a flame-retardant and fully recyclable mineral binder

Ronny Kürsteiner, Dan Vivas Glaser, Maximilian Ritter, Annapaola Parrilli, Jonas Garemark, Lorenza Maddalena, Thomas Schnider, Christopher H. Dreimol, Federico Carosio, Ingo Burgert, and Guido Panzarasa

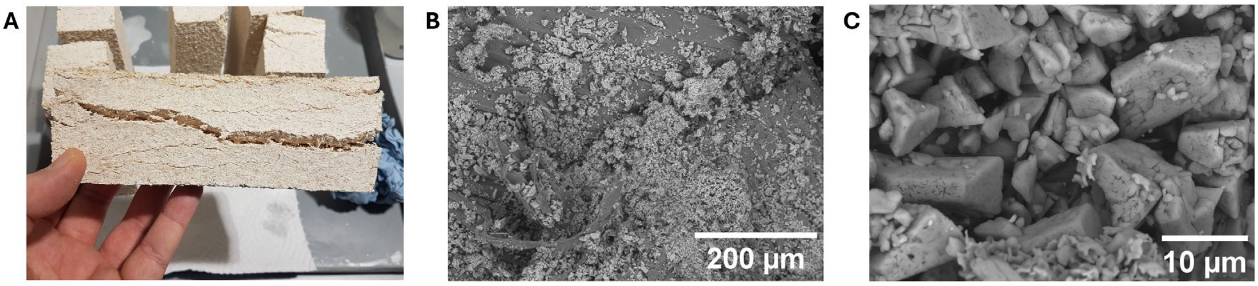

Figure S1. Control experiment with ammonium carbonate. (A) The use of ammonium carbonate as a source of NH_4^+ ions and to increase pH does not lead to consolidated sawdust-struvite composites. **(B)&(C)** Backscattered electron micrographs showed that struvite is precipitated in small (< 15 μm) crystallites.

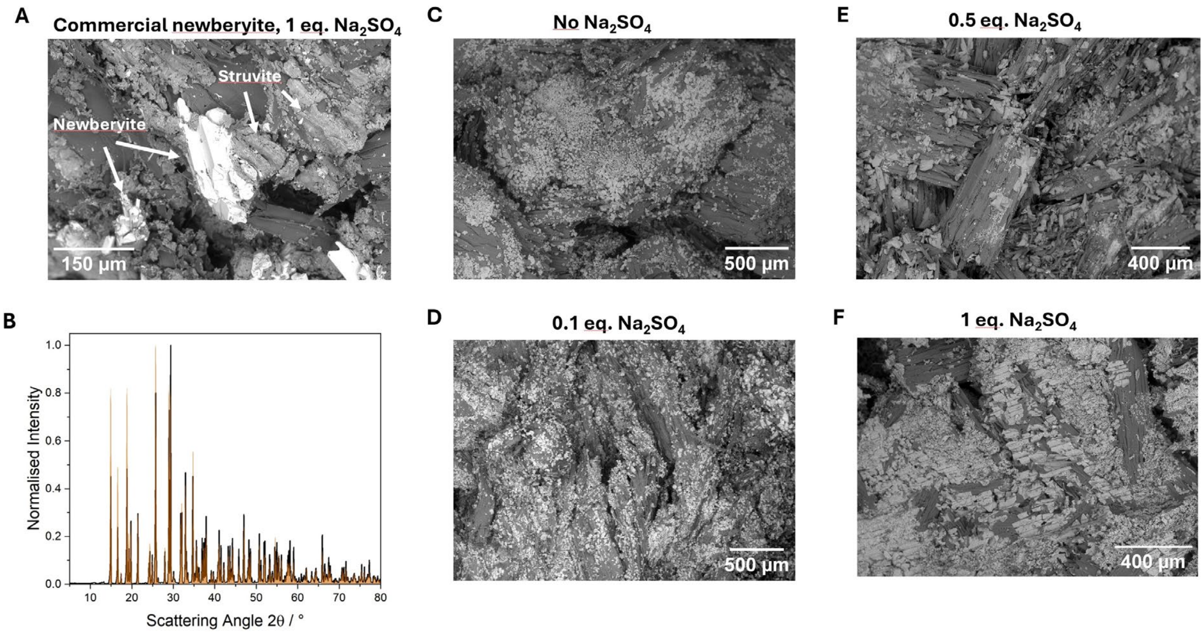

Figure S2. Influence of sodium sulfate concentration and size of newberyite on struvite crystallization. (A) Backscattered electron micrograph of the composite synthesized with commercial newberyite showed remaining newberyite due to the large (> 200 µm) crystallite sizes present. **(B)** The X-ray diffractogram of the synthesized precursor (black) showed that it is comprised of highly pure newberyite (orange, ICSD collection code 8228[1]). **(C)-(F)** Control experiments with various sodium sulfate concentrations showed an increase in the crystallite size of struvite with increasing sodium sulfate concentration.

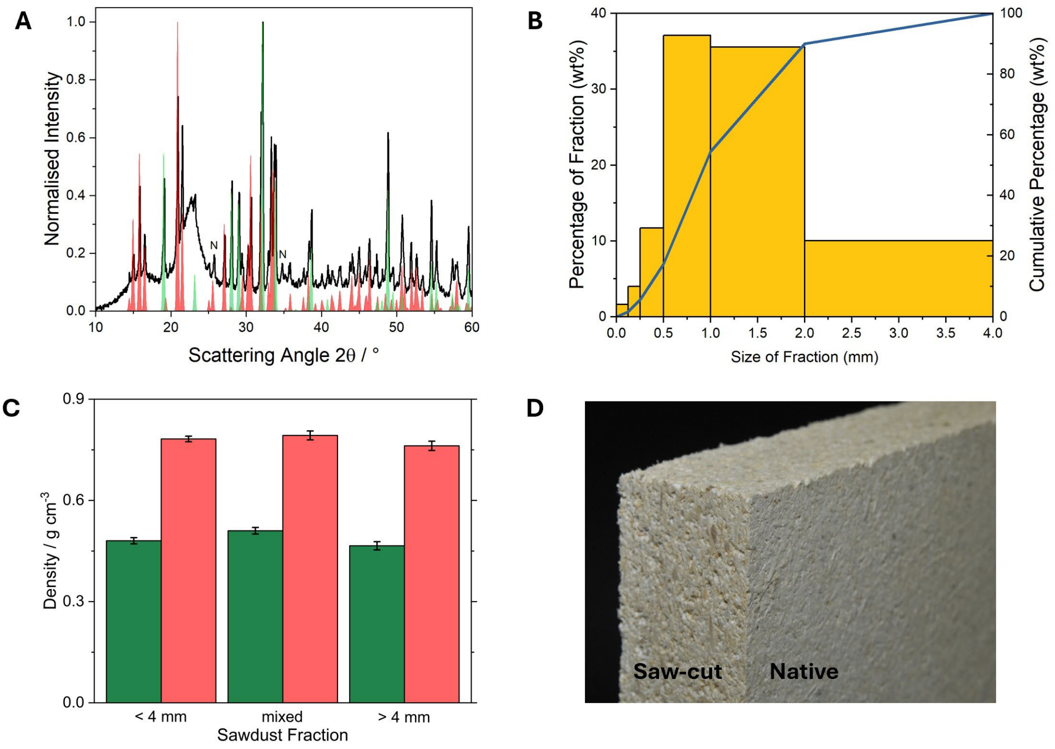

Figure S3. Macroscopic properties. (A) The diffractogram on 2 mm slices of the composite shows struvite (red, ICSD collection code 750[2]) and thénardite (green, ICSD collection code 2895[3]) to be the predominant inorganic phases. In addition, the reflections of the cellulose fibrils, and small amounts of unreacted newberyite (denoted 'N') are present. **(B)** Granulometry of the <4 mm sawdust fraction showed the majority of particles to be in the range of 0.5 – 2 mm. Most particles exhibited a high aspect ratio, some exceeding 10 mm in length. The > 4 mm sawdust fraction passed an 8 mm screen but was retained by a 4 mm screen. **(C)** The density of the composites is highly uniform across different sawdust fractions. **(D)** Photograph showing the as-synthesized and saw-cut surfaces. The composites were cut on a circular table saw with a carbide-tipped sawblade.

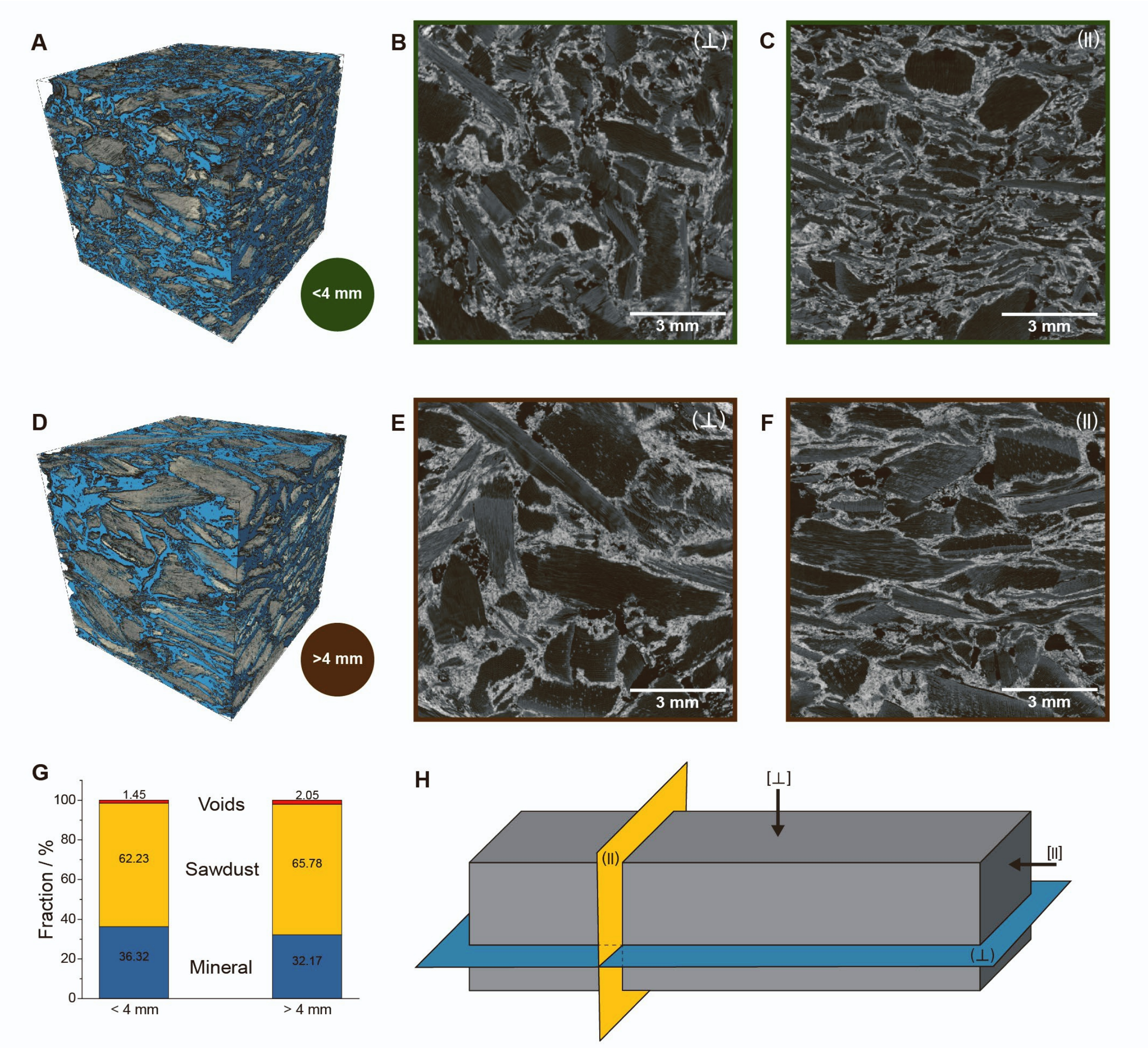

Figure S4. High resolution microtomography of high-density composites. Using specimens of ~12 mm edge length, a higher resolution with voxel size of 12 µm was achieved. **(A)-(C)** High density composite with < 4 mm sawdust fraction. **(D)-(F)** High density composite with > 4 mm sawdust fraction. **(A)&(D)** 3D reconstruction of the microtomography data with the inorganics colored in blue. **(B)&(E)** The sawdust particles are randomly oriented in (⊥). **(C)&(F)** In (‖), the texture of the sawdust particles is visible. **(G)** The higher mineral content and lower sawdust content of the composite with < 4 mm sawdust fraction can be attributed to the higher intermixing of mineral and sawdust resulting from the presence of fine wood particles. **(H)** Schematic representation of the convention used in this work. [⊥] is the direction of compaction during synthesis, [‖] denotes the long axis of the composites. (⊥) and (‖) denote planes normal to [⊥] and [‖], respectively.

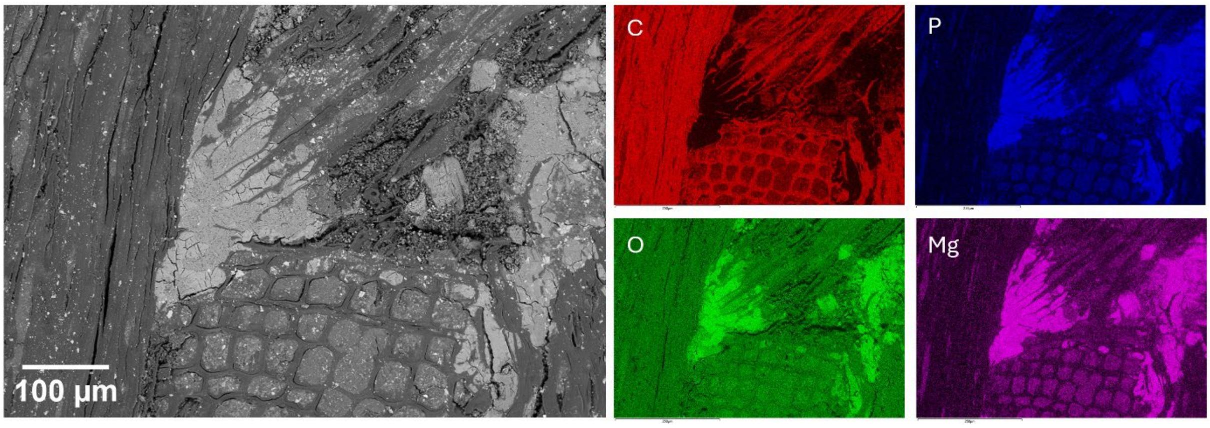

Figure S5. Microstructure and elemental analysis. Backscattered electron micrograph and elemental distribution maps for carbon, phosphorus, oxygen, and magnesium. The sample was polished using SiC abrasive media, which results in filled lumina of the cross section (lower middle) with sanding residue. The micrograph shows three sawdust particles of different orientation which are bonded by struvite. Noteworthy is that the struvite crystal grew into the accessible lumina of the sawdust particle in the upper right, leading to strong mechanical interlocking

Figure S6. Fracture behavior during mechanical tests. (A) Specimens after tensile tests in [||] (left) and [⊥] (right). Specimens loaded in [||] show a significantly higher roughness due to the orientation of the sawdust particles in direction of the load. Specimens loaded in [⊥] show a comparatively smooth fracture surface since the sawdust particles are oriented normal to the applied load. **(B)** Specimen after compression test in [||]. The specimen experiences high normal forces and failure predominantly occurs in [⊥]. **(C)** Characteristic stress-strain-curve for specimens compressed in [⊥]. The specimen is in a pseudo-elastic regime until ~8% strain, where it transitions into a second quasi-linear regime due to collapse of the sawdust fraction in the transversal directions, since Norway spruce has a compressive strength of ~4.2 MPa in the transversal directions[4]. At high strains > 30%, the composites undergo densification similar to native spruce. The inset shows the plastic deformation of the composites after compression to strains of 0.2 (left), 0.3 (middle), and 0.5 (right).

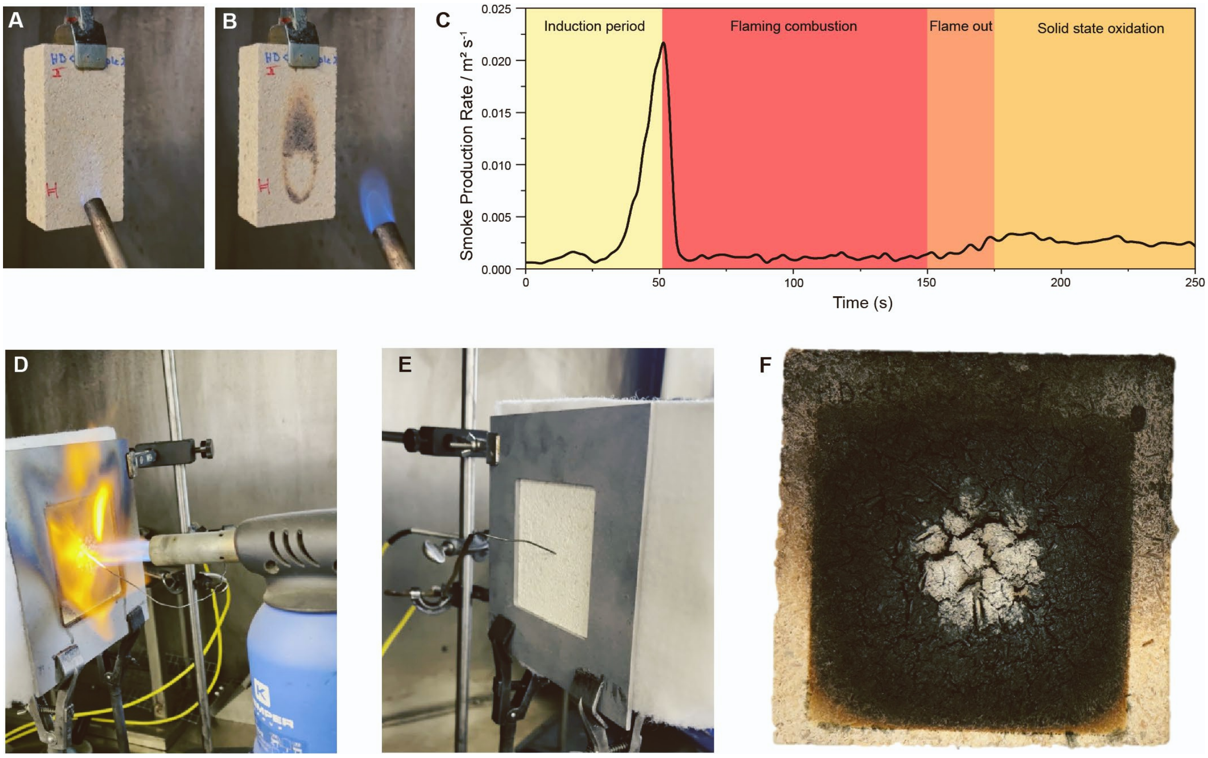

Figure S7. Flame retardant performance. (A) Specimen at the beginning of the flammability test with application of the flame on the surface of the specimen. **(B)** Specimen after the flammability test. **(C)** Smoke production rate during forced combustion measurement. **(D)** Front of the specimen during flame penetration test. **(E)** Back of the specimen after flame penetration test. **(F)** Front of the specimen after flame penetration test.

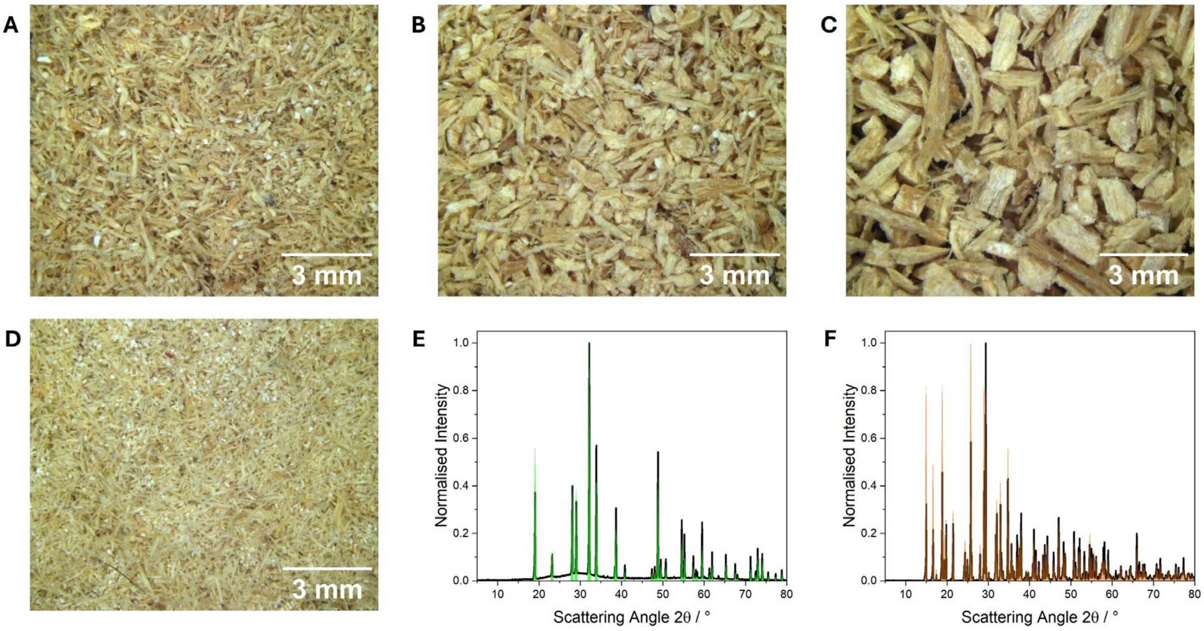

Figure S8. Recovery of mineral binder. (A)-(D) sawdust fraction after mechanical separation of inorganic material. **(E)** Diffractogram of thermally-decomposed inorganic binder (black) showing thénardite as the only crystalline phase remaining (green, ICSD collection code 2895[3]). **(F)** The X-ray diffractogram of the recovered newberyite (black) confirmed that it is of high purity (newberyite reference in orange, ICSD collection code 8228[1]).

References:

1. Abbona, F., Boistelle, R., and Haser, R. (1979). Hydrogen bonding in MgHPO4.3H2O (newberyite). Acta Crystallographica Section B *35*, 2514-2518.

2. Fugel, M., Malaspina, L.A., Pal, R., Thomas, S.P., Shi, M.W., Spackman, M.A., Sugimoto, K., and Grabowsky, S. (2019). Revisiting a Historical Concept by Using Quantum Crystallography: Are Phosphate, Sulfate and Perchlorate Anions Hypervalent? Chemistry – A European Journal *25*, 6523-6532.

3. Nord, A.G. (1973). Refinement of the Crystal Structure of Thenardite, Na2SO4. Acta Chemica Scandinavica *27*, 814-822.

4. Niemz, P., and Sonderegger, W. (2017). Festigkeitseigenschaften. In Holzphysik: Physik des Holzes und der Holzwerkstoffe, (Carl Hanser Verlag GmbH & Co. KG), pp. 336-414.